

## **Experimental methodology and analytical solution for cruciform ultrasonic fatigue testing**

Pedro R. da Costa<sup>1\*</sup>, Luís Reis<sup>1,2</sup>, Diogo Montalvão<sup>3</sup> and Manuel Freitas<sup>2,4</sup>

*<sup>1</sup>Instituto Superior Técnico, universidade de Lisboa, Av. Rovisco Pais, 1049-001 Lisbon, Portugal*

*<sup>2</sup>IDMEC, Instituto Superior Técnico, Av. Rovisco Pais, 1049-001 Lisbon, Portugal*

*<sup>3</sup>Department of Design and Engineering, Faculty of Science and Technology, Bournemouth University, Poole House, Talbot Campus, Fern Barrow, Poole BH12 5BB, United Kingdom*

*<sup>4</sup>Atlântica, Instituto Universitário, Fabrica da Pólvora, Barcarena, 2730-036 Barcarena, Portugal*

\* Corresponding author: pedro.r.costa@tecnico.ulisboa.pt

### **INTRODUCTION**

As transportation and general machinery demand higher working speeds, reliability, and life spans [1], a higher life span characterisation method was required. In the middle of the 20<sup>th</sup> century, Mason devised a new fatigue testing method very different from the established ‘conventional’. The designated ultrasonic fatigue machine utilises resonance principles to achieve a considerably higher testing frequency. With Mason’s generally accepted 20 kHz standard reaching a billion cycles was made reliable.

To make ultrasonic fatigue machines accessible and accepted, a trusted deterministic experimental methodology is necessary. Claude Bathias, the ultrasonic fatigue pioneer [1], brought ultrasonic fatigue testing (UFT) to the fatigue research world. His book details UTF methodology extensively for all uniaxial loading conditions [2]. Bathias et al. [3] have also shown piezoelectric fatigue testing machines in high and low temperatures, with  $R \neq -1$  stress ratios and fretting. Considerable worldwide research has followed Bathias well described and methodically presented methodologies [4]–[6].

The first ‘conventional’ fatigue machines focused on pure uniaxial cyclical load, meaning one single direction load. Multiaxial stresses were later recognised as the leading dynamic stress state in machines and structures [7]. Thereafter, several different multiaxial testing methods came to fruition over the years, replicating the different cyclic loads. Just as ‘conventional’ fatigue transposed from uniaxial to multiaxial testing mechanisms, UFT developments will follow the same trend. Palin Luc et al. [8] induced a biaxial bending stress state with a carefully shaped disk. P. Costa et al. [9] created an altered ultrasonic setup capable of inducing a specimen in a tension-torsion stress state.

In this study, a detailed methodology description with a proposed analytical solution is made to the already proven and working cruciform specimens created by D. Montalvão et al. [10]. Due to the cruciform deformation complexity, finite element analysis (FEA) was used to adjust Bathias analytical concepts.

## Cruciform ultrasonic fatigue

Three different geometries were put under FEA and experimentally measured under UFT conditions. The tested specimens and respective designations: Out-of-phase Compression-Tension samples (C-T); one only working as intended first tested in-phase Tension-Tension (F T-T); and new T-T design geometry (N T-T). Figure 1 presents the C-T and T-T specimens' deformed shape and the UFT booster-horn-specimen setup. Figure 1 also exhibits the followed coordinate x/y system to all made calculations. All three specimens were already under a first experimental analysis and FEA analysis by Costa et al. [11].

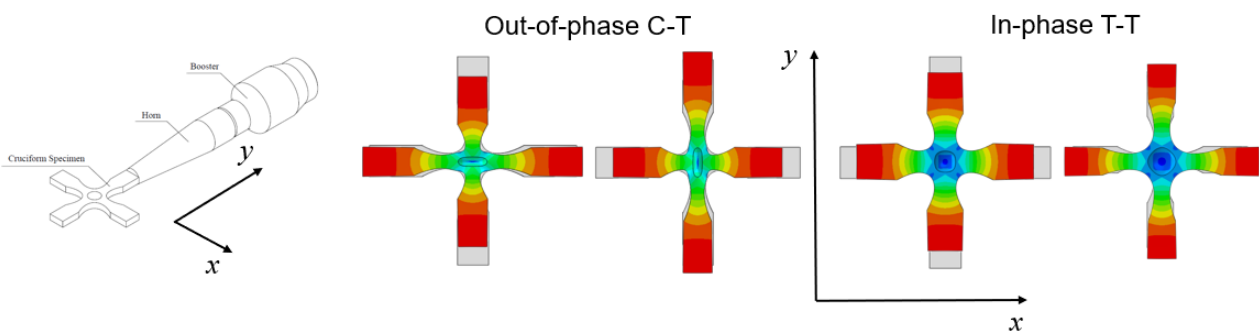


Fig 1. (A) Booster-horn-cruciform setup with the followed x/y coordinate system; (B) T-T and C-T resonant deformed shape (displacement magnitude)

## ANALYTICAL SOLUTION

The proposed analytical solution's main objective is to provide a deterministic process for the induced stress within the UFT measuring options. The Bathias uniaxial tension analytical solution method measures the highest displacement amplitude at the specimen's free base and determines its relation to the induced stress. The followed conception was to consider the cruciform geometry as two figurative perpendicular plane specimens with one shared fatigue testing region. The associated stress could then be determined by measuring the displacement at each cruciform arm's end (the free base of the figurative uniaxial specimens).

From careful cruciform geometry observation, two axial specimens' combinations are possible. These specimens were considered as 'Slices' ( $S_x$ ) made to the cruciform arms. Figure 2 shows the two possible 'slices' (S1 and S2) in a cruciform specimen with Bathias [2] axial specimens variable designations. Plane specimen defining dimensions were then associated with the followed Baptista et al. [12] cruciform dimensional variables.

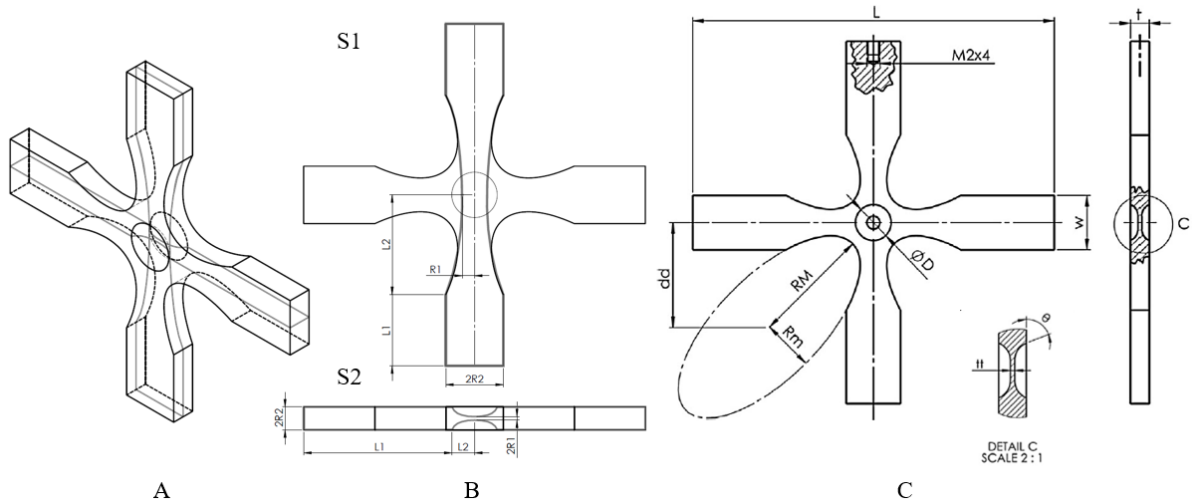


Fig 2. (A) Cruciform S1 and S2 3D cut representation; (B) S1 and S2 dimension variables; (C) Baptista et al. optimised geometry [12].

For S1 and S2 slices, one equivalent dimension needs to be determined:  $R_1$  for S1; and  $L_1$  for S2. The determined dimensions will ensure an equivalent 20 kHz uniaxial specimen.  $L_1$  for S2 is determined following Bathias methodology, just as an ordinary ultrasonic uniaxial specimen. For S1,  $R_1$  is iteratively determined by changing its value until the  $L_1$  length taken from the cruciform specimen is equal to the determined by Bathias methodology. Both S1 and S2 follow an exponential curvature.

From FEA, the cruciform arms stress distribution is not as straightforward as the uniaxial specimens overall distribution. Also, C-T and T-T specimen geometries show a considerable different stress distribution. Therefore, the S plane specimen is chosen according to the best stress gradient pairing for each cruciform. Figure 3 compares S 'slices' FEA obtained stress gradient results with the New T-T (N T-T) and C-T specimens. An approximation is also plotted for both presented specimens' results. The cruciform varying stress distribution tendency is associated with the complex deformation occurring in the specimen's connection between the arms. The irregular stress distribution was proven not influential on the maximum stress amplitude on the specimen by FEA analysis. Therefore, the made Approximation follows the stress distribution initial and final tendency.

The most similar slices to the cruciform arm's approximation behaviours are chosen from figure 3 plotted stress distributions. The T-T specimens follow the S1, while C-T specimens follow closer to the S2 slice. The still present stress distribution differences are then adjusted through Strain energy ( $U$ ). The energy input made by the ultrasonic setup will correspond to the total strain energy of the sample if no damping effects and connection friction between components are considered. Hence, the total Strain energy will be equal between cruciform arms and the S Slices. Since the S slices are designed from the cruciform, the same volume distribution as the cruciform arms can be considered.

If the volume distribution is equal and the total energy input is the same, the only variable difference is the stress distribution.

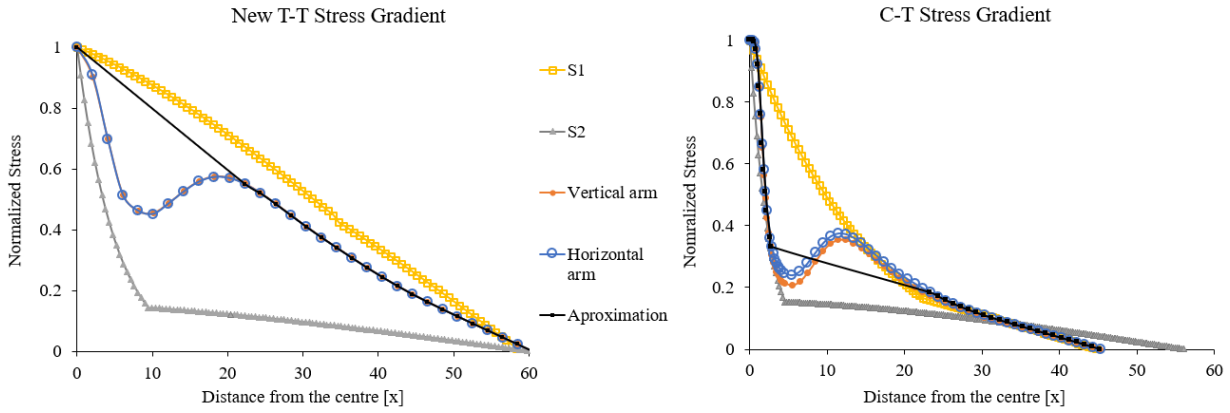


Fig 3. N T-T and C-T stress distribution of both vertical and horizontal arms, S1 and S2 slices; and Approximation

The strain energy correction is conducted through the stress distribution area. If the S stress area is higher or lower the strain energy is added or removed, respectively. The area difference compensation factor ( $\delta$ ) is then introduced in Bathias analytical solution. The resulted exponential equation (1) is as follows,

$$\begin{cases} \sigma(x) = E \cdot A_0 \cdot (1 + \delta) \cdot \varphi(L_1, L_2) [\beta \cosh(\beta x) - \alpha \sinh(\beta x)] \exp(-\alpha x), & \text{for } x \leq L_2 \\ \sigma(x) = E \cdot k \cdot A_0 \cdot (1 + \delta) \sin(k(L - x)) & , \text{for } L_2 < x \leq L \end{cases} \quad (1)$$

Where E is the materials Young Modulus and  $A_0$  is the measured displacement amplitude. Equation (1) is applied for both the  $x/y$  measured displacement amplitudes. The Hooke law is afterwards calculated for the determined midpoint stress ( $x=0; y=0$ ), thus having the biaxial stress state. However, as Costa et al. [11] perceived, all tested ultrasonic cruciform specimens exhibit a ‘flapping motion’ resulting in higher or lower  $x$  amplitude depending on the flap movement phase with the vertical arms  $y$  displacement. The associated motion is independent of the resonant mode being excited (T-T or C-T) and independent of the cruciform geometry. The proposed correction associates the  $x$ - $y$  amplitude difference and not the geometry itself. The designated ‘flapping’ motion factor ( $\gamma$ ) is then introduced in equations (1) and (2) by the area difference factor ( $\delta$ ). The flapping motion factor was determined empirically through measured amplitudes and strains of all tested geometries. Two different factors were empirically determined considering the ‘flapping’ motion phase. Equation (2) shows the flapping motion correction to be applied in accordance with the  $x$ - $y$  amplitude differences.

$$\begin{cases} \delta_{x,corrected} = \left( \delta - 1.75 \frac{A_{0x} - A_{0y}}{A_{0y}} \right), & \text{for } A_{0x} \geq A_{0y} \\ \delta_{x,corrected} = \left( \delta - 0.75 \frac{A_{0x} - A_{0y}}{A_{0y}} \right), & \text{for } A_{0x} \leq A_{0y} \end{cases} \quad (2)$$

## RESULTS AND DISCUSSION

Experimental measurements were made to all three mentioned ultrasonic cruciform specimens. Simultaneous  $x$  and  $y$  displacement measurements were conducted at the horizontal and vertical arms, respectively. Roseate strain gauges were attached to the cruciform midpoint aligned with the axial-axial directions. Through Hooke's law, the measured strains were transformed into induced biaxial stress.

Detailed analysis of all cruciform strain results and measured displacements show a low-stress difference between  $x/y$  but a significant difference in displacement. The difference is associated with the flapping motion, showing a higher  $x$  amplitude when  $y$  is in-phase with the associated flapping motion displacements and lower in out-of-phase. The biaxial stress state was then calculated from the  $x$  and  $y$  displacements following the proposed analytical solution methodology. Figure 4 compares the strain gauge determined stress with the analytically calculated stress.

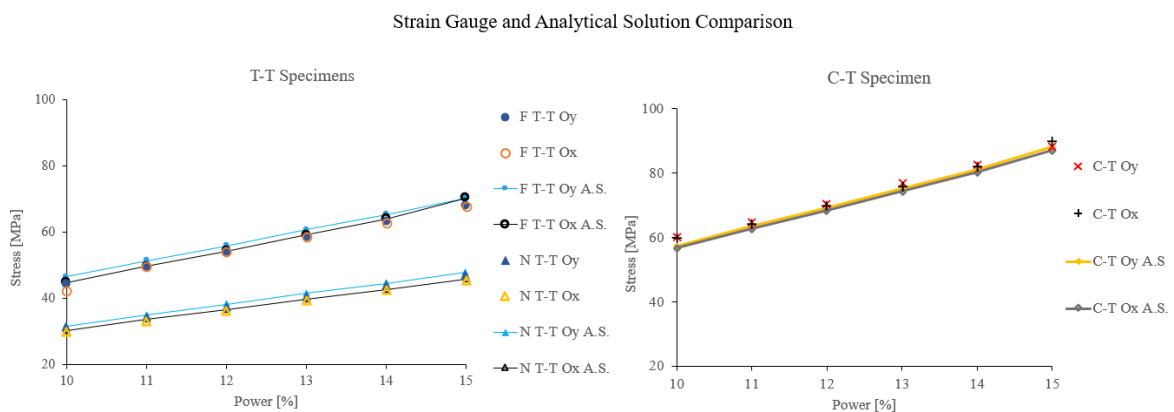


Fig 4. Comparison between strain gauge calculated stress and analytical solution stress (A.S.).

The proposed analytical solution showed a low correlation error with the strain measurements. For every tested cruciform in two different horn setups, a maximum average difference of 5% was obtained. There was only one exception where an N T-T  $x$  stress presented close to a 9% stress difference. The error could be associated with the strain gauge's alignment error due to its small size or/and the gauge area strain measurement instead of a central point.

## CONCLUSIONS

A proposed analytical solution was reached through a careful transformation of Bathias uniaxial solution. The followed base concept from uniaxial to cruciform analytical conversion considered cruciform geometries and mode shape deformation parallel to two perpendicular uniaxial specimens with one shared centre region.

Three different cruciform geometries were experimentally tested to complete and verify the proposed analytical solution. FEA analysis of the three cruciform geometries showed that their behaviour was not fully parallel to the figurative uniaxial specimens. A first correction adjustment was achieved by strain energy differences, the area difference compensation factor ( $\delta$ ). A second correction factor was determined experimentally associated with the exhibit 'flapping' motion on the horizontal arms. The associated displacements were proven negligible to the final induced stress, but they influence the measured displacement amplitude. The proposed 'flapping' motion factor ( $\gamma$ ) was empirically determined, independent of cruciform geometry.

Lastly, the proposed analytical solution was calculated. The biaxial stress state was then compared to the measured by roseate strain gauges. A lower 5% error average was observed in all tested samples, with only close x stress 9% error exception on an N T-T specimen.

## ACKNOWLEDGMENTS

This work was supported by FCT, through IDMEC, under LAETA, project UID/EMS/50022/2019. Financial support from Portuguese Fundação para a Ciência e Tecnologia (FCT) is acknowledged through project PTDC/EMS- PRO/5760/2014.

## REFERENCES

- [1] H. Mughrabi and S. D. Antolovich, *Int. J. Fatigue*, 2016, vol. 93, pp. 217–223.
- [2] C. Bathias and P. C. Paris, *Gigacycle fatigue in mechanical practice*. 2005.
- [3] C. Bathias, *Int. J. Fatigue*, 2006, vol. 28, no. 11, pp. 1438–1445.
- [4] H. Q. Xue, H. Tao, F. Montembault, Q. Y. Wang, and C. Bathias, *Int. J. Fatigue*, 2007, vol. 29, pp. 2085–2093.
- [5] M. Vieira, et al., *Frat. ed Integrita Strutt.*, 2016, vol. 10, no. 37, pp. 131–137.
- [6] M. Freitas, V. Anes, and D. Montalvao, *An. Mecânica la Fract.*, 2011, vol. 1, no. 28, pp. 335–340, [Online]. Available: <http://uhra.herts.ac.uk/ha>.
- [7] M. de Freitas, *Theor. Appl. Fract. Mech.*, 2017, vol. 92, no. May, pp. 360–372.
- [8] C. Brugger, T. Palin-Luc, P. Osmond, and M. Blanc, *Procedia Struct. Integr.*, 2016, vol. 2, pp. 1179–1180.
- [9] P. Costa, et al., *Int. J. Fatigue*, 2017, vol. 103, pp. 248–257.
- [10] D. Montalvão and A. Wren, *Heliyon*, 2017, vol. 3, no. 11, p. e00466.
- [11] P. R. da Costa, et al., *Fatigue Fract. Eng. Mater. Struct.*, 2019, vol. 42, no. 11, pp. 2496–2508.
- [12] R. Baptista, et al., *Theor. Appl. Fract. Mech.*, 2015, vol. 80, pp. 65–72.